

# Reconstruction of 3-D Symmetric Curves from Perspective Images without Discrete Features

Wei Hong<sup>1</sup>, Yi Ma<sup>1</sup>, and Yizhou Yu<sup>2</sup>

<sup>1</sup> Department of Electrical and Computer Engineering

<sup>2</sup> Department of Computer Science

University of Illinois at Urbana-Champaign

Urbana, IL, 61801, USA

{weihong, yima, yyz}@uiuc.edu

**Abstract.** The shapes of many natural and man-made objects have curved contours. The images of such contours usually do not have sufficient distinctive features to apply conventional feature-based reconstruction algorithms. This paper shows that both the shape of curves in 3-D space and the camera poses can be accurately reconstructed from their perspective images with unknown point correspondences given that the curves have certain invariant properties such as symmetry. We show that in such cases the minimum number of views needed for a solution is remarkably small: one for planar curves and two for nonplanar curves (of arbitrary shapes), which is significantly less than what is required by most existing algorithms for general curves. Our solutions rely on minimizing the  $L^2$ -distance between the shapes of the curves reconstructed via the “epipolar geometry” of symmetric curves. Both simulations and experiments on real images are presented to demonstrate the effectiveness of our approach.

## 1 Introduction

One of the main thrusts of research in computer vision is to study how to reconstruct the shapes of 3-D objects from (perspective) images. Depending on the choice of the models for the shape (e.g., surfaces, volumes, or points), the reconstruction methods differ. On one hand, surface- and volume-based approaches are excellent for reconstructing free-form objects, but typically require precise precalibrated camera poses and sufficient variations (texture or shading) on the surfaces to achieve accurate reconstruction. On the other hand, when the objects (or scene) have discrete feature points (or lines), camera poses, calibration and the 3-D structures can be simultaneously recovered from the images via the well-established methods in multiple-view geometry [1, 2].

Nevertheless, free-form natural or man-made objects with curved contours are ubiquitous in the real world, and very often their images do not have sufficient texture or feature points for us to apply conventional algorithms to accurately recover the surfaces and camera poses. So what can we do when we need to recover such curved shapes as well as camera poses from images without enough feature points to start with? In general, this is a very daunting task and in fact an impossible one unless certain constraints are imposed on either the shapes or the camera motions.

In this paper, we show that if the shape boundary consists of *symmetric curves*, the shape of the curves and the camera poses are strongly encoded in the perspective images and can be recovered accurately from as few as two images – via the “epipolar geometry” of symmetric curves. All that is needed is the correspondence between entire curves, and no prior correspondences between points on the curves are required.

Furthermore, if the symmetric curves in space are planar, both the shape of the curves and the camera pose can be recovered uniquely from a single view.

**Relation to prior work.** While multiple-view geometry of points, lines, and planes have been extensively studied and well-understood, recent studies have gradually turned to use curves and surfaces as basic geometric primitives for modeling and reconstructing 3-D shapes. The difficulty in reconstruction of curves is that the point correspondences between curves are not directly available from the images because there are no distinct features on curves except the endpoints. An algorithm in [3] was proposed to automatically match individual curves between images using both photometric and geometric information. The techniques introduced in [4, 5] aimed to recover the motion and structure for arbitrary curves from monocular sequences of images. It was realized that it is not possible to uniquely and accurately reconstruct both the shape and camera poses for an arbitrary 3-D curve from an arbitrary set of views. Therefore, some restrictions need to be put on the views and curves themselves to guarantee a unique reconstruction. It was shown that, under circular motions, curved objects can be recovered from their silhouettes or contours [6–9]. The algorithm given in [10] can reconstruct symmetric shapes made of generalized cylinders. Reconstruction of curves from multiple views based on affine shape method was studied in [11, 12]. The reconstruction of algebraic curves from multiple views has been proposed by [13, 14].

This paper introduces symmetry as a very effective constraint to solve the reconstruction problem for 3-D curves. Such methods are very useful in practice since symmetric curves are ubiquitous in a wide range of natural and man-made scenes (e.g., leaves, signs, containers). Symmetry has long been exploited as a very effective cue in feature-based reconstruction methods [15–19]. Our work generalizes such methods to feature-less smooth curves.

**Contribution of this paper.** In this paper, we propose a novel approach for the reconstruction of curves in space and the recovery of camera poses by imposing global symmetry constraints on the original shapes of the curves. As part of the derivation, we establish the precise conditions and minimal number of views required for a unique solution: a) there is always a two-parameter family of ambiguous solutions in reconstructing general symmetric curves from a single view; b) nevertheless if the curves are planar (in space), the solution becomes unique; c) for general symmetric curves, two generic views are sufficient to give a unique solution (summarized in Table 1).

## 2 Symmetric Curve Representation

### 2.1 Perspective Image of a Curve

A parameterized curve  $\gamma(t)$  in  $\mathbb{R}^n$  with parameter  $t \in [t_a, t_b]$  is a continuous map

$$\gamma(\cdot) : t \mapsto \gamma(t) \in \mathbb{R}^n, \quad t \in [t_a, t_b]. \quad (1)$$

A curve  $\gamma$  is an equivalence class of parameterized curves because a curve can be arbitrarily parameterized. Two parameterized curves  $\gamma_1, \gamma_2$  are said to be equivalent if there exists a continuous, monotonically increasing reparameterization function  $\sigma : t \mapsto t'$  such that

$$\gamma_1(t) = \gamma_2(\sigma(t)). \quad (2)$$

The image of a 3-D parameterized curve  $\Gamma(t)$  in  $\mathbb{R}^3$ ,  $t \in [t_a, t_b]$  taken at  $g_0 = (R_0, T_0)$  is a 2-D parameterized curve  $\gamma(s)$  in  $\mathbb{R}^2$  with parameter  $s \in [s_a, s_b]$ .  $s =$

$\sigma(t)$  is a reparameterization of  $t$ . If the camera is calibrated, the image curve  $\gamma(s)$  in homogeneous image coordinates and the space curve  $\Gamma(t)$  in spatial coordinates are related by

$$\lambda(s)\gamma(s) = \Pi_0 g_0 \Gamma(t), \quad (3)$$

where  $s = \sigma(t)$ ,  $s_a = \sigma(t_a)$ ,  $s_b = \sigma(t_b)$ , and  $\Pi_0 = [I, 0]$  is the standard projection matrix. The parameter  $s, t$  may be the same, i.e. the reparameterization  $\sigma$  can be an identity function, which however we do not assume to know at this point.

## 2.2 Image of Symmetric Curves

Now we consider a pair of curves  $\Gamma, \Gamma'$  that are reflectively symmetric to each other with respect to a central plane  $P_r$ .<sup>3</sup> Without loss of generality, we assume that the two curves are symmetric with respect to the  $yz$ -plane of a selected canonical coordinate frame. The reflection can be represented by a Euclidean motion  $g_r = (R_r, 0)$ , where

$$R_r \doteq \begin{bmatrix} -1 & 0 & 0 \\ 0 & 1 & 0 \\ 0 & 0 & 1 \end{bmatrix} \in O(3) \subset \mathbb{R}^{3 \times 3}. \quad (4)$$

Then  $\Gamma'(t) = g_r \Gamma(t)$ . If one image of the symmetric curves is taken at  $g_0 = (R_0, T_0)$ , the images of the two curves are:

$$\lambda(s)\gamma(s) = \Pi_0 g_0 \Gamma(t), \quad \lambda'(s')\gamma'(s') = \Pi_0 g_0 g_r \Gamma(t), \quad (5)$$

where  $s = \sigma(t)$ ,  $s_a = \sigma(t_a)$ ,  $s_b = \sigma(t_b)$  and  $s' = \sigma'(t)$ ,  $s'_a = \sigma'(t_a)$ ,  $s'_b = \sigma'(t_b)$ .

## 2.3 Corresponding Points and Epipolar Geometry of Symmetric Curves

Notice that we can rewrite the equation for the image of the second curve as

$$\lambda'(s')\gamma'(s') = \Pi_0 g_0 g_r g_0^{-1} (g_0 \Gamma(t)).$$

Therefore, the image of the two symmetric curves can be interpreted as two images of the same curve taken with a relative camera pose

$$g_0 g_r g_0^{-1} = (R, T) \doteq (R_0 R_r R_0^T, R_0 R_r T_0).$$

Under this interpretation, the two images ( $\gamma(s), \gamma'(s')$ ) of the pair of points ( $\Gamma(t), \Gamma'(t)$ ) become the two images of a single point  $\Gamma(t)$  in space taken from two different views. These corresponding image points should satisfy the epipolar constraint

$$\gamma'(s')^T \widehat{T} R \gamma(s) = 0, \quad \forall s \in [s_a, s_b], \quad s' \in [s'_a, s'_b], \quad \sigma^{-1}(s) = \sigma'^{-1}(s'), \quad (6)$$

where we use  $\widehat{T}$  to indicate the skew-symmetric matrix associated to  $T$  such that  $\widehat{T}v = T \times v$  for all  $v \in \mathbb{R}^3$ . From the definition of  $R_r, R$  and  $T$ , it is not difficult to show that  $\widehat{T}R = \widehat{T}$ . Hence the above epipolar constraint is simplified to:

$$\gamma'(s')^T \widehat{T} \gamma(s) = \gamma'(s')^T \widehat{\gamma(s)} T = 0, \quad \sigma^{-1}(s) = \sigma'^{-1}(s'). \quad (7)$$

We call  $T$  the ‘‘vanishing point’’ for the pair of symmetric curves since it is parallel to the line defined by each pair of corresponding points ( $\Gamma(t), \Gamma'(t)$ ).

The two reparameterization  $\sigma(\cdot)$  and  $\sigma'(\cdot)$  can be made the same in the following *polar coordinates* for the pair of curves. If the vanishing point  $T \in \mathbb{R}^3$  is known<sup>4</sup>,

<sup>3</sup> In this paper, we work primarily with reflective symmetry. But the same method, with some modification, can be applied to curves with translational or rotational symmetry.

<sup>4</sup>  $T$  is in homogeneous coordinates and  $\|T\| = 1$ .

the intersection of the two image curves  $\gamma$  and  $\gamma'$  with any ray through  $T$  are two corresponding image points<sup>5</sup>. The angle of the ray  $\theta$  and the distance to the vanishing point  $T$  establish the polar coordinates. The angle  $\theta$  becomes a suitable parameter for the two curves so that  $\gamma(\theta)$  and  $\gamma'(\theta)$  are always two corresponding symmetric points. The epipolar constraint in polar coordinates becomes

$$\gamma'(\theta)^T \widehat{\gamma(\theta)} T = 0, \quad \forall \theta \in [\theta_a, \theta_b]. \quad (8)$$

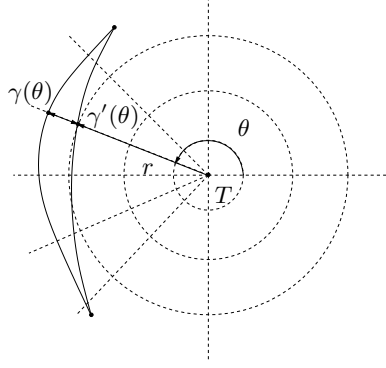


**Fig. 1.** Corresponding points can be easily obtained for a pair of symmetric curves in polar coordinates  $(r, \theta)$ .

### 3 Reconstruction of Symmetric Curves from Images

#### 3.1 Ambiguity in Reconstruction of Symmetric Curves from a Single View

There are essentially three different cases for the image of a pair of symmetric curves that we illustrate in Figure 2. When the two pairs of end points of  $\gamma$  and  $\gamma'$  are separate as in case (a), the vanishing point  $T$  is uniquely determined and so is the correspondence between points on the two image curves. In the remaining cases (b) and (c), extra constraints need to be imposed on the symmetric curves sought in order to have a unique solution. We will focus on case (c) which is the most general case.

As illustrated in Figure 3, if the actual vanishing point  $T$  is given, the 3-D depths for each pair of corresponding points in image can be uniquely determined via the following “triangulation” equation [15]:

$$\begin{bmatrix} \widehat{T}\gamma(\theta) & -\widehat{T}\gamma'(\theta) \\ T^T\gamma(\theta) & T^T\gamma'(\theta) \end{bmatrix} \begin{bmatrix} \lambda(\theta) \\ \lambda'(\theta) \end{bmatrix} = \begin{bmatrix} 0_{3 \times 1} \\ 2d \end{bmatrix}, \quad (9)$$

where  $d$  is the distance from the camera center to the symmetry plane  $P_r$ . The first row of this equation means that  $T$  is the vanishing point of the family of parallel lines

<sup>5</sup> Using polar coordinates is convenient when there is only one intersection between a ray and an image curve. However, when there are multiple intersections, the correspondences among the intersections with a known  $T$  should be set up as follows. Suppose the sequence of intersections with curve  $\gamma$  is  $\{p_0, p_1, \dots, p_m\}$ , and the sequence of intersections with curve  $\gamma'$  is  $\{q_0, q_1, \dots, q_n\}$ . Then  $m = n$ , and  $p_i$  corresponds to  $q_{m-i}$ .

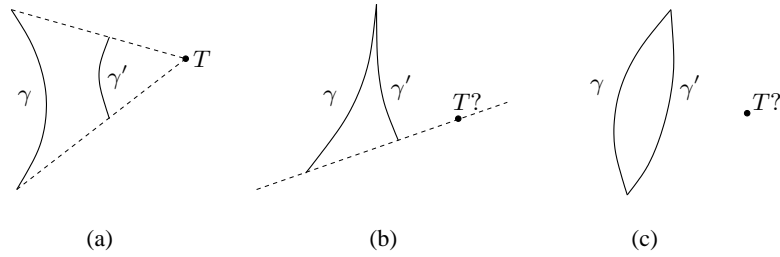


**Fig. 2.** (a)  $T$  is uniquely determined by the two pairs of end points; (b)  $T$  is determined by one pair of end points up to a line; (c)  $T$  is a two-parameter family.

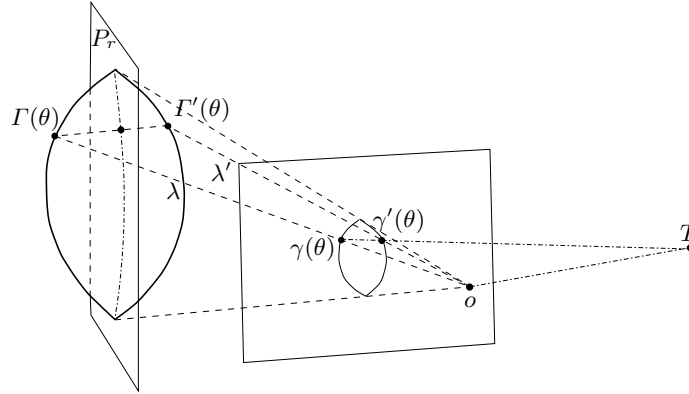


**Fig. 3.** If the vanishing point  $T$  is given, the 3-D depths for each pair of corresponding points in image can be uniquely determined.

between  $\Gamma(\theta)$  and  $\Gamma'(\theta)$ . The line  $oT$  is parallel to the family of lines  $\Gamma(\theta)\Gamma'(\theta)$  in 3-D. The second row of the equation implies that the distances from the points  $\Gamma(\theta)$ ,  $\Gamma'(\theta)$  to the symmetry plane  $P_r$  are equal. However, if the correct  $T$  is not known, the above equation always has a unique solution for  $\lambda(\theta)$  and  $\lambda'(\theta)$  for an arbitrarily chosen  $T$ . Furthermore the recovered 3-D curves  $\Gamma(\theta) = \lambda(\theta)\gamma(\theta)$  and  $\Gamma'(\theta) = \lambda'(\theta)\gamma'(\theta)$  are indeed symmetric. We hence have proven the following lemma:

**Lemma 1.** *Given a pair of curves  $\gamma$  and  $\gamma'$  on the image plane and an arbitrary feasible vanishing point  $T$ , there exists a pair of curves in space  $\Gamma$  and  $\Gamma'$  such that  $\gamma$  and  $\gamma'$  are their images, respectively.*

Lemma 1 states an unfortunate fact: for the pair of 2-D image curves shown in Figure 1, almost any choice of the vanishing point  $T$  results in a valid 3-D interpretation of the curves as the image of some pair of symmetric curves in 3-D. Therefore, for case (c) of Figure 2, there is a two-parameter family of pairs of symmetric curves in 3-D that give rise to the same pair of image curves; for case (b), there is a one-parameter family.

### 3.2 Reconstruction of Planar Symmetric Curves from a Single View

From the above discussions, the reconstruction of a pair of general symmetric curves from a single view is in general an *ill-posed* problem,<sup>6</sup> unless some additional conditions are imposed upon the class of curves of interest. Most symmetric curves in practice are planar curves, and we first examine if this additional information may lead to a unique solution.

For the pair of planar symmetric curves in case (c) of Figure 2, the central line  $l_c$  of the curves in the image is determined by connecting the two end points.<sup>7</sup> As before, the true vanishing point  $T$  leads to a correspondence of the two curves. Let  $\gamma(\theta)$ ,  $\gamma'(\theta)$  and  $l_c(\theta)$  be corresponding points on the two curves and the central line. Also,  $l_c$  should lie on the central plane  $P_r$ . With the additional planar constraints, Equation (9) gives rise to

$$\begin{bmatrix} \widehat{T}\gamma(\theta) & -\widehat{T}\gamma'(\theta) & 0_{3 \times 1} \\ T^T\gamma(\theta) & T^T\gamma'(\theta) & 0 \\ \gamma(\theta) & \gamma'(\theta) & -2l_c(\theta) \end{bmatrix} \begin{bmatrix} \lambda(\theta) \\ \lambda'(\theta) \\ \lambda_c(\theta) \end{bmatrix} = \begin{bmatrix} 0_{3 \times 1} \\ 2d \\ 0_{3 \times 1} \end{bmatrix}, \quad \forall \theta \in [\theta_a, \theta_b]. \quad (10)$$

After eliminating  $\lambda_c(\theta)$  by multiplying  $\widehat{l}_c(\theta)$  on both sides of the third row, the equation becomes

$$\begin{bmatrix} \widehat{T}\gamma(\theta) & -\widehat{T}\gamma'(\theta) \\ T^T\gamma(\theta) & T^T\gamma'(\theta) \\ \widehat{l}_c(\theta)\gamma(\theta) & \widehat{l}_c(\theta)\gamma'(\theta) \end{bmatrix} \begin{bmatrix} \lambda(\theta) \\ \lambda'(\theta) \end{bmatrix} = \begin{bmatrix} 0_{3 \times 1} \\ 2d \\ 0_{3 \times 1} \end{bmatrix}, \quad \forall \theta \in [\theta_a, \theta_b]. \quad (11)$$

This equation can be rewritten as

$$\begin{bmatrix} \widehat{T}\gamma(\theta) & -\widehat{T}\gamma'(\theta) & 0_{3 \times 1} \\ T^T\gamma(\theta) & T^T\gamma'(\theta) & 2d \\ \widehat{l}_c(\theta)\gamma(\theta) & \widehat{l}_c(\theta)\gamma'(\theta) & 0_{3 \times 1} \end{bmatrix} \begin{bmatrix} \lambda(\theta) \\ \lambda'(\theta) \\ 1 \end{bmatrix} \doteq M(T, \theta)\Lambda(\theta) = [0_{7 \times 1}], \quad \forall \theta \in [\theta_a, \theta_b]. \quad (12)$$

The *necessary condition* for a valid solution of  $T$  for planar symmetric curves is

$$\boxed{\text{rank}[M(T, \theta)] = 2, \quad \forall \theta \in [\theta_a, \theta_b].} \quad (13)$$

Since only the correct vanishing point  $T$  can satisfy the above rank condition, a criterion for finding the correct  $T$  is

$$T = \arg(\text{rank}[M(T, \theta)] = 2), \quad \forall \theta \in [\theta_a, \theta_b]. \quad (14)$$

Once  $T$  is found, the depth vector  $\Lambda$  can also be obtained as

$$\Lambda(\theta) = \text{null}(M(T, \theta)). \quad (15)$$

In practice, the rank condition will not be exactly satisfied by any  $T$  due to noise. We may choose  $\Lambda(\theta)$  to be the eigenvector of  $M(T, \theta)$  that is associated with the smallest eigenvalue. So we want to find the  $T$  such that  $\int_{\theta_a}^{\theta_b} \|M(T, \theta)\Lambda(\theta)\|^2 d\theta$  is minimized. Let the singular value decomposition (SVD) of the matrix  $M$  be  $M(T, \theta) = U(T, \theta)\Sigma(T, \theta)V(T, \theta)^T$ ,

<sup>6</sup> Except for the special case (a) of Figure 2.

<sup>7</sup> For case (b), the image of the central line can also be determined from  $\gamma$  and  $\gamma'$  and we here do not elaborate due to the limit of space.

$$T = \arg \min \left( \int_{\theta_a}^{\theta_b} \|M(T, \theta)\Lambda(\theta)\|^2 d\theta \right) = \arg \min \left( \int_{\theta_a}^{\theta_b} \Sigma_{3,3}(T, \theta)^2 d\theta \right), \quad (16)$$

where  $\Sigma_{3,3}$  is the smallest singular value of  $M$ . Once  $T$  is found, the depth vector  $\Lambda$  is recovered as the third column of  $V(T, \theta)$ . In Section 4, we will show how this simple criterion gives accurate reconstruction of planar symmetric curves.

### 3.3 Reconstruction of General Symmetric Curves from Two Views

For a pair of general symmetric curves, according to Lemma 1, a single view is not enough for a unique recovery. In this subsection, we show that how an extra view may resolve this problem.

As an example, Figure 4 illustrates two images of a pair of (reflectively) symmetric curves. If  $T_1$  and  $T_2$  are the correct vanishing points in the two image planes, the images

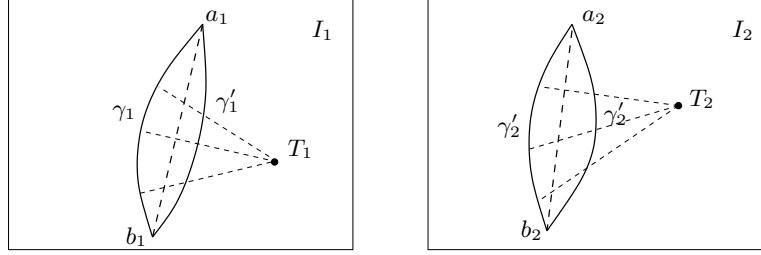


**Fig. 4.** Two images of a pair of symmetric curves. Assume that  $(R_{21}, T_{21})$  is the relative motion from the first view to the second.  $T_1$  and  $T_2$  are the vanishing points of the two images, respectively.

of the curves satisfy the two equations:

$$\begin{aligned} \begin{bmatrix} \widehat{T}_1 \gamma_1(\theta_1) & -\widehat{T}_1 \gamma_1'(\theta_1) \\ T_1^T \gamma_1(\theta_1) & T_1^T \gamma_1'(\theta_1) \end{bmatrix} \begin{bmatrix} \lambda_1(\theta_1) \\ \lambda_1'(\theta_1) \end{bmatrix} &= \begin{bmatrix} 0_{3 \times 1} \\ 2d_1 \end{bmatrix}, \quad \forall \theta_1 \in [\theta_a, \theta_b]. \\ \begin{bmatrix} \widehat{T}_2 \gamma_2(\theta_2) & -\widehat{T}_2 \gamma_2'(\theta_2) \\ T_2^T \gamma_2(\theta_2) & T_2^T \gamma_2'(\theta_2) \end{bmatrix} \begin{bmatrix} \lambda_2(\theta_2) \\ \lambda_2'(\theta_2) \end{bmatrix} &= \begin{bmatrix} 0_{3 \times 1} \\ 2d_2 \end{bmatrix}, \quad \forall \theta_2 \in [\theta_a, \theta_b]. \end{aligned} \quad (17)$$

For simplicity, we typically choose  $d_1 = d_2 = 1/2$  at this moment. The correct relative scale between  $d_1$  and  $d_2$  can be determined at a later stage. Given any two vanishing points  $T_1$  and  $T_2$ , from Lemma 1, the above triangulation equations in general have solutions for  $[\lambda_1(\theta_1), \lambda_1'(\theta_1)]$  and  $[\lambda_2(\theta_2), \lambda_2'(\theta_2)]$ . We thus obtain two pairs of symmetric 3-D curve  $[I_1(\theta_1), I_1'(\theta_1)]$  and  $[I_2(\theta_2), I_2'(\theta_2)]$  via triangulation.  $[I_1(\theta_1), I_1'(\theta_1)]$  and  $[I_2(\theta_2), I_2'(\theta_2)]$  are in the two camera coordinates of the two views. If  $T_1$  and  $T_2$  are the correct vanishing points, the reconstructed curves are all related to the same pair of 3-D symmetric curves  $\Gamma$  and  $\Gamma' = g_r \Gamma$  in space via the rigid transformations  $g_{01} = (R_{01}, T_{01})$  and  $g_{02} = (R_{02}, T_{02})$  (the two camera poses), respectively,

$$\begin{aligned} I_1(\theta_1) &= g_{01} \Gamma(\theta_1), & I_1'(\theta_1) &= g_{01} g_r \Gamma(\theta_1), \\ I_2(\theta_2) &= g_{02} \Gamma(\theta_2), & I_2'(\theta_2) &= g_{02} g_r \Gamma(\theta_2). \end{aligned} \quad (18)$$

The distance between the end points of the curves should be preserved under rigid transformations. So the correct ratio between  $d_1$  and  $d_2$  can be determined as

$$\frac{d_1}{d_2} = \frac{\|F_1(\theta_{a1}) - F_1(\theta_{b1})\|}{\|F_2(\theta_{a2}) - F_2(\theta_{b2})\|} = \frac{\|l_{c1}\|}{\|l_{c2}\|}. \quad (19)$$

With respect to each view, the canonical pose  $g_0$  of the curves can be recovered from symmetry as follows. Because the vanishing point  $T$  is orthogonal to the central plane,  $T$  can be chosen as the  $x$ -axis of the canonical frame; the central line  $l_c = F(\theta_a) - F(\theta_b)$  is chosen to be the  $y$ -axis since it is in the central plane; an endpoint, say for example  $F(\theta_a)$ , can be selected to be the origin of the canonical frame. Then the  $R_0$  can be retrieved as

$$R_0 = \left[ T, \frac{l_c}{\|l_c\|}, \hat{T} \frac{l_c}{\|l_c\|} \right] \in \mathbb{R}^{3 \times 3}, \quad T_0 = F(\theta_a) \in \mathbb{R}^3. \quad (20)$$

From either  $F_1$  or  $F_2$ , the 3-D curves in the canonical frame,  $F_{01}$  or  $F_{02}$  respectively, can be recovered. According to the Lemma 1, all possible  $T_1$  and  $T_2$  in the two image planes can generate two sets of curves  $F_{01}(T_1)$  and  $F_{02}(T_2)$ . If the vanishing points  $T_1$  and  $T_2$  are correct,  $F_{01}$  and  $F_{02}$  should be identical. Therefore, the true curve  $F$  is the intersection of the two sets. This gives the necessary condition for the correct vanishing points,

$$\boxed{[T_1, T_2] = \arg(F_{01}(T_1) = F_{02}(T_2))}. \quad (21)$$

For real images with noise, the equality may not be achieved. The following optimization criterion can be used to find  $T_1, T_2$  by minimizing

$$[T_1, T_2] = \arg \min (\text{distance}(F_{01}(T_1), F_{02}(T_2))). \quad (22)$$

There are many different choices in the distance between two curves. We use the simplest Euclidean distance, also known in functional analysis as the  $L^2$ -distance:<sup>8</sup>

$$\text{distance}(F_1, F_2) \doteq \int_{t_a}^{t_b} \|F_1(t) - F_2(t)\|^2 dt, \quad (23)$$

where  $F_1$  and  $F_2$  are both parameterized by their arc length  $t$ . Notice that the above criterion is rather different from most curve reconstruction algorithms that are based on minimizing the reprojection error in the images via the notion of ‘‘bundle-adjustment’’ (e.g., see [11]). The above method minimizes the discrepancy in the shapes of the reconstructed 3-D curves in space. Furthermore, the method can be easily generalized if *multiple images* of the same curves are given.

The optimal  $T_1$  and  $T_2$  can be found via any nonlinear optimization scheme chosen at the user’s discretion.<sup>9</sup> For case (b) of Figure 2, the vanishing points will lie on the line generated by the two separate end points. So the search for  $T_1$  and  $T_2$  is two-dimensional. For case (c) of Figure 2, each  $T_1$  and  $T_2$  is two dimensional, and therefore the search is in a four-dimensional space. For curves with general shapes, the solution is always unique.

To conclude Section 3, we summarize all cases of symmetric curves studied so far in Table 1, in terms of ambiguities in reconstruction from one or two views.

<sup>8</sup> We have also tried other distances such as  $L^1$ -distance and  $C^1$ -distance. They all give similar reconstruction results for the simulations and experiments conducted in this paper.

<sup>9</sup> For the simulations and experiments given in this paper, we used the simple MATLAB function ‘‘fminsearch.’’ We observed standard convergence rate from such an off-the-shelf nonlinear optimization toolbox. The convergence rate may be improved with a custom-designed algorithm and initialization.



| # of solutions | General curves |          |          | Planar curves |
|----------------|----------------|----------|----------|---------------|
|                | case (a)       | case (b) | case (c) |               |
| One view       | unique         | 1-family | 2-family | unique        |
| Two views      | unique         | unique   | unique   | unique        |

**Table 1.** Ambiguity in reconstruction of symmetric curves: A single view is not enough for reconstruction of general symmetric curves, except for case (a) of Figure 2, but sufficient for planar symmetric curves. Two or more views are needed for reconstruction of generally shaped symmetric curves.

## 4 Experimental Results

### 4.1 Simulations

**One view of planar curves.** To test the performance of the proposed methods, we have conducted extensive simulations. In the first simulation, a pair of planar 3-D symmetric curves in case (c) of Figure 2 are generated. A perspective image of their curves is obtained from a pin-hole camera model. In order to test the robustness of our algorithm, 5% asymmetry is added onto the 3-D symmetric curves<sup>10</sup> and white Gaussian noise is added to the projected image curves with standard deviation  $\sigma$ . The added noise corresponds to approximately one pixel in standard deviation for a 400x320 pixel image. A large variety of view points are tested. From the simulations, we found that the view angle  $\alpha$  between the camera optical axis and the central plane  $P_r$  is the most important factor for the accuracy in reconstruction. The Table 2 shows the error as a function of the angle  $\alpha$ . Only the angles from  $+10^\circ$  to  $+70^\circ$  are tested because the negative side will give similar results due to symmetry. The shape error is the  $L^2$ -distance between the curves reconstructed and the ground truth.<sup>11</sup> The camera pose error is the angle (in degrees) between the original camera rotation matrix and the rotation matrix reconstructed. The results indicate that the shape error and the camera pose error increase with an increasing angle  $\alpha$ . However, even in the worst case, the errors remain very small, which indicates that our method is quite effective.

| view angle $\alpha$ (degree)   | 10     | 20     | 30     | 40     | 50     | 60     | 70     | 80     |
|--------------------------------|--------|--------|--------|--------|--------|--------|--------|--------|
| shape error ( $L^2$ -distance) | 0.0170 | 0.0168 | 0.0223 | 0.0264 | 0.0271 | 0.0320 | 0.0361 | 0.0375 |
| camera pose error (degree)     | 0.2529 | 0.5571 | 0.5090 | 0.3193 | 0.3275 | 0.3916 | 0.5066 | 1.2401 |

**Table 2.** The error of the shape and camera pose as a function of the view angle  $\alpha$  between the camera axis and the central plane. It indicates that the shape error and the camera pose error in general increase when the angle  $\alpha$  is increasing.

**Two views of general curves.** In the second simulation, a pair of non-planar 3-D curves in case (c) of Figure 2 is generated, and two images are obtained from two view points. A large variety of view points are tested. It is discovered from the simulation results that the relative view angle  $\alpha' = |\alpha_1 - \alpha_2|$  (difference in the angles between the two camera axes and the central plane) is the most important factor. Only the angles from  $10^\circ$  to  $60^\circ$

<sup>10</sup> We make the curves slightly asymmetric by adding to the curves deformation of a magnitude up to 5% of the maximum distance between the two curves.

<sup>11</sup> The length of the curves is always normalized to be one for comparison.

are tested because other angles will result in similar results due to symmetry. Table 3 shows the error as a function of the angle  $\alpha'$ . The shape error is the distance between the curves reconstructed from the noisy images and the ground truth. The results indicate that the shape error and the camera pose error in general decrease with the increasing of the relative view angle  $\alpha'$ . However, all of these errors remain small.

| relative view angle $\alpha'$ (degree) | 10     | 20     | 30     | 40     | 50     | 60     |
|--|--------|--------|--------|--------|--------|--------|
| shape error ( $L^2$ -distance)         | 0.0253 | 0.0228 | 0.0264 | 0.0221 | 0.0245 | 0.0203 |
| average camera pose error (degree)     | 3.8600 | 4.4582 | 3.7642 | 3.2266 | 3.8470 | 3.4047 |

**Table 3.** The error of the shape and camera pose as a function of the relative view angle  $\alpha'$  between the two camera axes. It indicates that the shape error and the camera pose error in general decrease when the angle  $\alpha'$  increases.

## 4.2 Experiments on Real Images

Figure 5 shows an example of a reconstructed umbrella. This example belongs to the case (b) of Figure 2. The whole umbrella can be reconstructed from a single image using the two-view method because the stripes on the umbrella are all identical and two stripes in one view can be treated as two views of the same stripe.

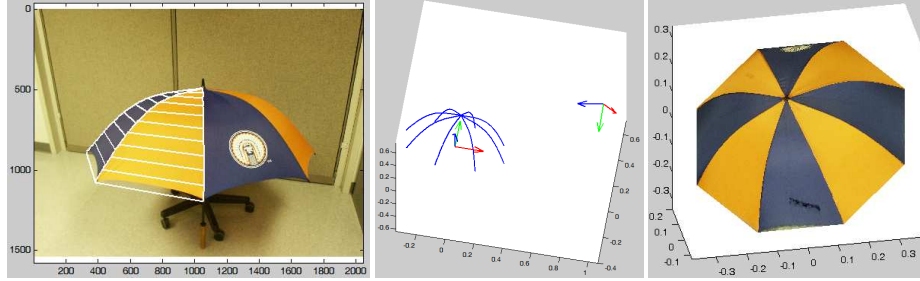


**Fig. 5.** Left: A single image that is used to recover the whole umbrella. The vanishing lines obtained from the optimization are shown in the image. Middle: The frame of the umbrella recovered from two stripes. Right: A synthetically rendered view of the completely reconstructed umbrella from the top.

Figure 6 shows an example of leaves whose contours can be considered as planar curves, which is in the category of Figure 2 (c). The recovered structures as well as a synthetically rendered image of the reconstructed leaves are shown. This experiment verifies that from only one single view, the structure of symmetric planar curves can be recovered accurately.

Figure 7 shows a reconstruction of a 3-D leaf from two views. It is an example of general curves in the category of Figure 2 (c). The recovered structure as well as a synthetically rendered image of the reconstructed leaf are shown. We can see that the shape of the leaf has been convincingly recovered.

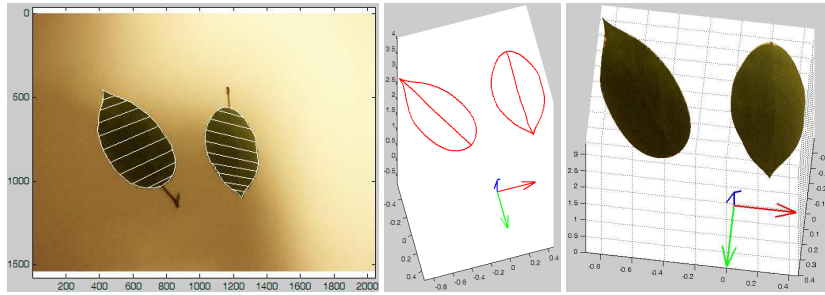


**Fig. 6.** Left: A single image that is used to recover the leaves. The vanishing lines obtained from the optimization are shown in the image. Middle: The shape of the leaf boundaries and the camera pose recovered from the image. Right: A synthetically rendered image of the reconstructed leaves.

On a Pentium III 866MHz computer with MATLAB 6.0, the algorithm completes in 5 minutes for the one-view examples and 10 minutes for the two-view examples.

## 5 Conclusions and Future Work

In this paper, we have provided simple and effective algorithms for the simultaneous reconstruction of both the shape of smooth symmetric curves and the camera poses from as few as one or two images without feature correspondences to start with. Both simulations and experiments show that the results are remarkably accurate. In the future, we plan to combine our methods with surface techniques for symmetric shape reconstruction. We will also study the effects of various deformations on the reconstruction of such shapes.

## References

1. Faugeras, O.: Three-Dimensional Computer Vision, A geometric approach. MIT Press (1993)
2. Hartley, R., Zisserman, A.: Multiple View Geometry in Computer Vision. Cambridge University Press (2003)
3. Schmid, C., Zisserman, A.: The geometry and matching of curves in multiple views. In: European Conference on Computer Vision. (1998)
4. Papadopoulo, T., Faugeras, O.: Computing structure and motion of general 3D curves from monocular sequences of perspective images. In: European Conference on Computer Vision. (1996)
5. Papadopoulo, T., Faugeras, O.: Computing structure and motion of general 3D curves from monocular sequences of perspective images. Technical Report 2765, INRIA (1995)
6. Wong, K.Y.K., Cipolla, R.: Structure and motion from silhouettes. In: 8th IEEE International Conference on Computer Vision. Volume II., Vancouver, Canada (2001) 217–222
7. Mendonça, P.R.S., Wong, K.Y.K., Cipolla, R.: Camera pose estimation and reconstruction from image profiles under circular motion. In: European Conference on Computer Vision. Volume II. (2000) 864–877
8. Cipolla, R., Blake, A.: Surface shape from the deformation of apparent contours. In: IEEE International Conference on Computer Vision. (1992) 83–112
9. G. Cross, A.W.F., Zisserman, A.: Parallax geometry of smooth surfaces in multiple views. In: IEEE International Conference on Computer Vision. (1999) 323–329

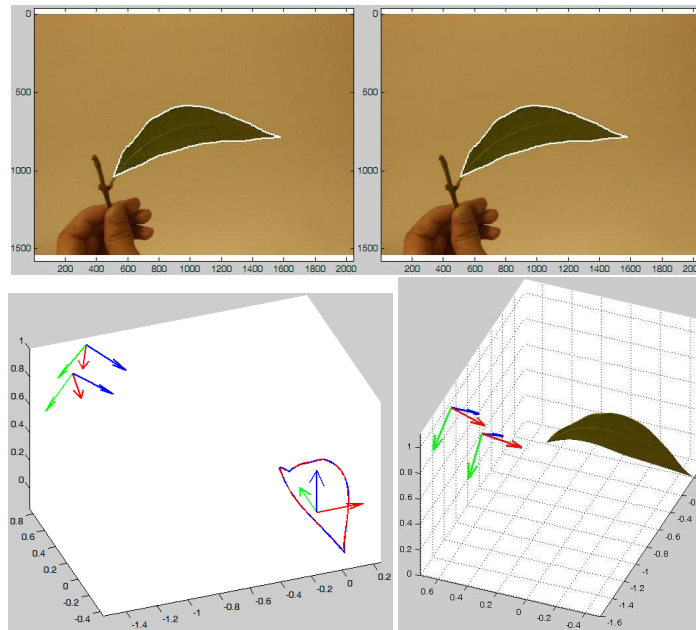


**Fig. 7.** Top: Two images that are used to recover a nonplanar leaf. Bottom Left: The shape of the leaf boundary and camera poses recovered from the two views (note that the difference between the two recovered boundaries is almost indistinguishable). Bottom Right: A synthetically rendered image of the reconstructed leaf.

10. François, A., Medioni, G.G.: A human-assisted system to build 3-D models from a single image. In: IEEE International Conference on Multimedia Computing and Systems. (1999) 282–288
11. Berthilsson, R., Astrom, K., Heyden, A.: Reconstruction of curves in  $\mathbb{R}^3$ , using factorization and bundle adjustment. In: IEEE International Conference on Computer Vision. (1999)
12. Berthilsson, R., Astrom, K.: Reconstruction of 3D-curves from 2D-images using affine shape methods for curves. In: International Conference on Computer Vision and Pattern Recognition. (1997)
13. Kaminski, J., M.Fryers, Shashua, A., Teicher, M.: Multiple view geometry of non-planar algebraic curves. In: IEEE International Conference on Computer Vision. (2001)
14. Kaminski, J., Shashua, A.: On calibration and reconstruction from planar curves. In: European Conference on Computer Vision. (2000)
15. Hong, W.: Geometry and reconstruction from spatial symmetry. Master Thesis, UIUC (2003)
16. Hong, W., Yang, A.Y., Ma, Y.: On symmetry: Structure, pose and calibration from a single image. International Journal on Computer Vision (Submitted 2002)
17. Mitumoto, H., Tamura, S., Okazaki, K., Fukui, Y.: 3-D reconstruction using mirror images based on a plane symmetry recovering method. IEEE Transactions on Pattern Analysis and Machine Intelligence **14** (1992) 941–946
18. Zabrodsky, H., Weinshall, D.: Using bilateral symmetry to improve 3D reconstruction from image sequences. Computer Vision and Image Understanding **67** (1997) 48–57
19. Zabrodsky, H., Peleg, S., Avnir, D.: Symmetry as a continuous feature. IEEE Transactions on Pattern Analysis and Machine Intelligence **17** (1995) 1154–1166